URSI GASS 2021, Rome, Italy, 28 August - 4 September 2021

Axial Ring Feed Horn with Logarithmic Flare for Offset Gregorian Optics

Doug Henke*(1), Sara Salem Hesari (1), and Lewis B. G. Knee (1)
(1) NRC Herzberg Astronomy and Astrophysics Research Centre, Victoria, BC V9E 2E7, Canada

Abstract

We present an improved axial ring feed horn using a logarithmic spiral flare opening and tapered groove geometry that is suitable for wide-angle feeding, as required for offset Gregorian telescopes. To enable a design with maximum aperture efficiency, full 2-D field integration was calculated as part of the optimization loop. Since aperture efficiency includes the contributions of cross-polarization, phase, amplitude, and taper, directly optimizing against these terms will result in excellent wideband performance. An example design is shown and optimized for the 30–51 GHz band.

1 Telescope Optics and Feed Parameters

Both SKA and ngVLA have adopted offset Gregorian telescope optics, in part, to achieve high efficiency with an unblocked primary [1]–[3].

For more than a decade, the Dominion Radio Observatory (DRAO) has been developing carbon fibre composite technology that is ideal for the reflectors used in large offset dual-reflector telescopes. The DVA series of telescopes are recent technology demonstrators, and DVA-1 employs a 15-m projected primary aperture, as shown in Figure 1 [4]–[7].

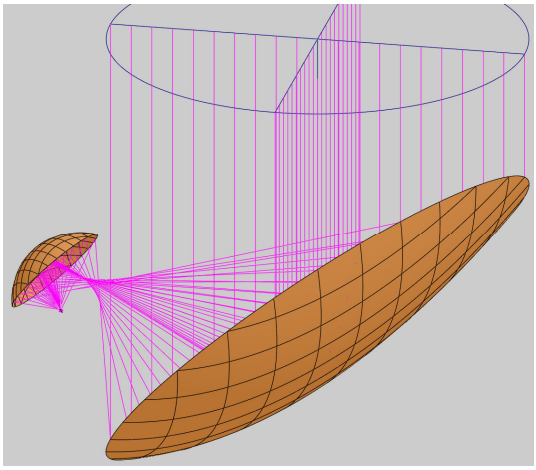

Figure 1. CAD model of the reflectors used on the DVA-1 telescope. Shaped offset Gregorian optics are used and optimized to receive a feed with a half angle of 55° and edge taper of 16 dB on the secondary. The primary has a projected aperture of 15 m.

Similar to SKA and ngVLA, the ideal feed for DVA-1 has a frequency independent half-angle of 55° corresponding to an edge taper of 16 dB. The shaping of the secondary provides an optimal edge taper on the primary of ~11 dB [4], [5].

2 Proposed Feed and Optimization Procedure

Axial ring groove feed horns are ideally suited for wide beam widths and can achieve excellent performance as shown in [8], [9]. Figure 2 shows the approach where an additional flaring section is added to the throat of the horn, along with variation of the rings and grooves to enable thicker, more machinable features. It is assumed that the feed will be machined on a lathe.

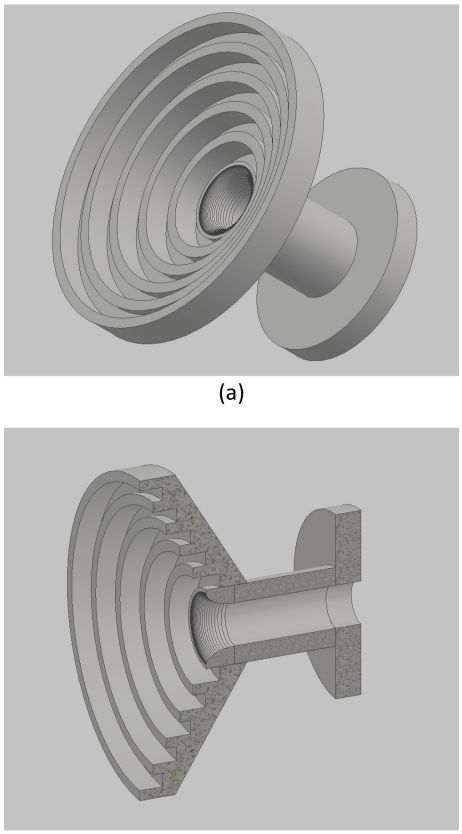

Figure 2. (a) CAD model of an axial ring feed horn. (b) Section view of the horn showing the logarithmic spiral cross-section of the inner guide.

The flaring of the inner guide follows the radius of a logarithmic spiral:

$$\rho = K * e^{\alpha \cdot \varphi} \qquad (1)$$

where K is a scaling constant, α is the rate of decay, and φ is the polar angle (in Figure 2, a ¼-turn of a full revolution is used and K = 200 and α = -1.77).

A number of axial rings and grooves are used to give uniformity to the beam and provide a constant field taper at the desired feed angle. In the example shown in Figure 2, five rings are used to provide a compromise between performance and physical size. The leading edges of the rings follow a simple opening angle (60.6° in Figure 2), while the groove depths have a slight taper that become shallower at the outermost groove. For a given pitch between successive rings, the ring width is approximately 0.43**pitch*. The feed horn waveguide diameter is 6.7 mm.

Since a primary goal of the offset Gregorian optics is to increase overall efficiency, a full 2-D integrated aperture efficiency calculation was used to drive the goal function of the optimizer.

The spill-over, amplitude, phase, and polarization efficiencies shown here have been calculated according to [10]:

$$\eta_{spill} = \frac{\int_0^{2\pi}\int_0^{\theta_m}(|\boldsymbol{E}_{co}|^2+|\boldsymbol{E}_{cross}|^2)sin\theta d\theta d\phi}{\int_0^{2\pi}\int_0^{\pi}(|\boldsymbol{E}_{co}|^2+|\boldsymbol{E}_{cross}|^2)sin\theta d\theta d\phi}, \qquad (2)$$

$$\eta_{amp} = \frac{\left[\int_0^{2\pi}\int_0^{\theta_m}(|\boldsymbol{E}_{co}|)sin\theta d\theta d\phi\right]^2}{\left[\int_0^{2\pi}\int_0^{\theta_m}(|\boldsymbol{E}_{co}|^2)sin\theta d\theta d\phi\right]\cdot\left[\int_0^{2\pi}\int_0^{\theta_m} sin\theta d\theta d\phi\right]}, \qquad (3)$$

$$\eta_{pol} = \frac{\int_0^{2\pi}\int_0^{\theta_m}(|\boldsymbol{E}_{co}|^2)sin\theta d\theta d\phi}{\int_0^{2\pi}\int_0^{\theta_m}(|\boldsymbol{E}_{co}|^2+|\boldsymbol{E}_{cross}|^2)sin\theta d\theta d\phi}, \qquad (4)$$

$$\eta_{phase} = \left(\frac{\left|\int_0^{2\pi}\int_0^{\theta_m}(\boldsymbol{E}_{co})sin\theta d\theta d\phi\right|}{\int_0^{2\pi}\int_0^{\theta_m}(|\boldsymbol{E}_{co}|)sin\theta d\theta d\phi}\right)^2, \qquad (5)$$

where $\boldsymbol{E}_{co}$ and $\boldsymbol{E}_{cross}$ are, respectively, the co- and cross-polarized electric far fields projected onto a spherical grid, θ_m is the half-angle integration limit representing the reflector rim boundary of the equivalent paraboloid, and

$$\eta_{ap,far-field} = \eta_{spill} \cdot \eta_{amp} \cdot \eta_{pol} \cdot \eta_{phase}. \qquad (6)$$

The EM model of the horn was solved within CST Microwave Studio, but launched via Matlab's COM server function *actserver*. As shown in Figure 3, Matlab's multi-variable Nelder-Mead optimizer (*fminsearch*) was used to drive the optimization loop. The far-fields were exported as a source file (*.ffs) along with the S-parameters. On completion of the CST solver, the far-fields and S-parameters were read into Matlab and the aperture efficiency was calculated according to (2)–(6).

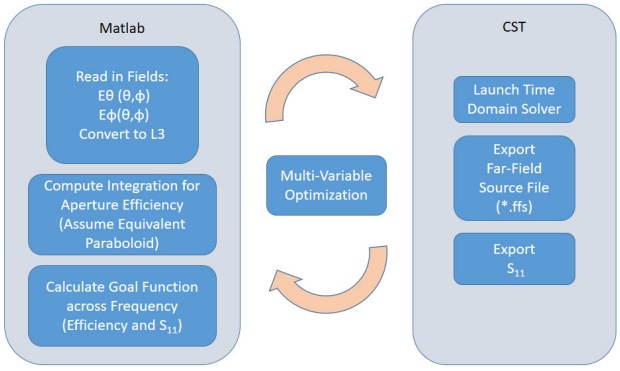

Figure 3. Optimisation loop used to drive feed horn design. The CST model was launched within Matlab code and later used to calculate the aperture efficiency as part of the overall goal function.

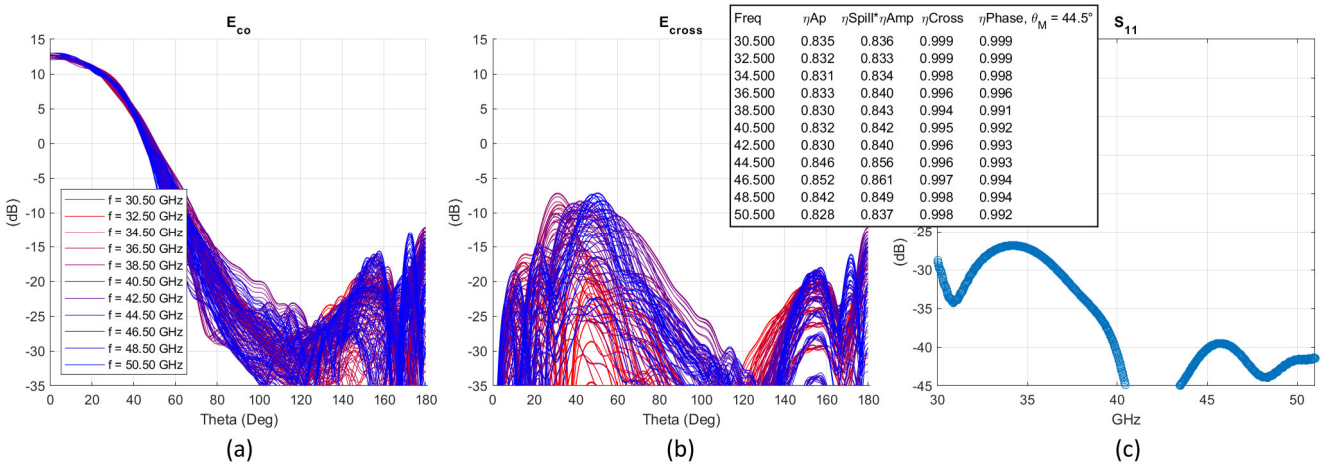

Freq	ηAp	ηSpill*ηAmp	ηCross	ηPhase, θM = 44.5°
30.500	0.835	0.836	0.999	0.999
32.500	0.832	0.833	0.999	0.999
34.500	0.831	0.834	0.998	0.998
36.500	0.833	0.840	0.996	0.996
38.500	0.830	0.843	0.994	0.991
40.500	0.832	0.842	0.995	0.992
42.500	0.830	0.840	0.996	0.993
44.500	0.846	0.856	0.996	0.993
46.500	0.852	0.861	0.997	0.994
48.500	0.842	0.849	0.998	0.994
50.500	0.828	0.837	0.998	0.992

Figure 4. Optimized performance of the feed horn shown in Figure 2. (a) Co-polar field cuts along φ=0°, 5°, 10°, …, 360° are overlaid across the full frequency band demonstrating constant beamwidth and circularly symmetric beams. (b) Cross-polar field cuts across frequency. (c) Reflected power response. (Inset) Table showing calculated aperture efficiency terms. The column entitled η_{Ap} is the aperture efficiency product as given by (6).

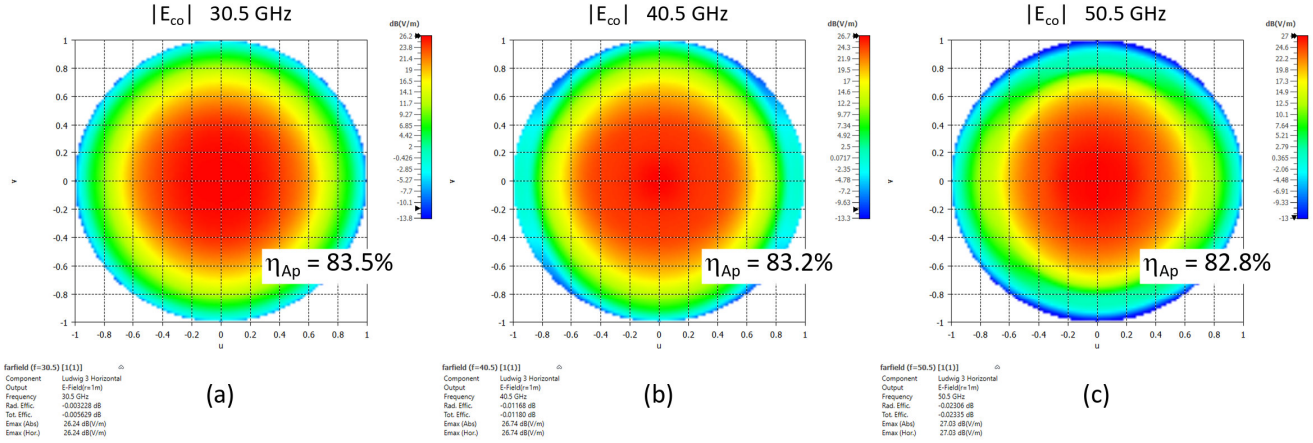

Figure 5. Co-polar far-field amplitude response plotted in the u-v plane for (a) 30.5 GHz, (b) 40.5 GHz, and (c) 50.5 GHz. A 40 dB colour scale is used for all plots and demonstrates the uniformity and circularly symmetric beams across the band.

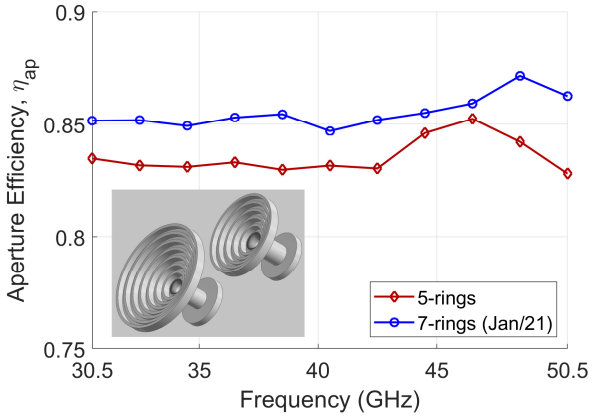

Figure 6. Comparison of the aperture efficiency improvement when increasing the number of axial rings on the feed horn from 5 to 7 rings [11]. The aperture diameters are 5.0 and 6.6 cm respectively.

As a simplification step, an equivalent paraboloid representation was used [10]. Using a Gaussian feed through the DVA-1 optics, it was empirically determined that an equivalent paraboloid using a half-angle of 44.5° approximates a 55°, 16 dB edge taper feed through the dual-reflector shaped optics. I.e., $\theta_m = 44.5°$ was used to estimate the aperture efficiency for the shaped optics of Figure 1.

Figure 4 shows the optimized far-fields for the logarithmic flare axial ring feed horn. In (a), the co-polar electric field cuts are overlaid across the frequency band indicating constant beam width and circular symmetry. Figure 4 (b) shows the cross-polar field component and (c) shows the reflected power response (-25 dB was considered sufficient during optimization). The table inset to Figure 4 displays the calculated efficiency terms according to (2)–(6) and shows that an estimated aperture efficiency of 83% was obtained. Phase efficiency was calculated assuming a fixed physical phase centre location across the band (here set at 1.5 mm from the start of the spiral flare), demonstrating over 99% phase efficiency. Polarization efficiency was shown to ~99.5% over the band.

Figure 5 also shows a 2-D mapping of the co-polar field in the u-v plane that illustrates constant edge taper across frequency.

This technique lends itself to weighting individual aperture efficiency terms within the goal function to enhance particular specifications, e.g., phase uniformity or polarization purity. Further gains in overall efficiency can be realized using more axial rings. Figure 6 shows an example of an optimized 7-ring feed horn, used in [11], demonstrating ~85% aperture efficiency across the band.

Future work will include optimization refinement, reducing cross-polarization, and validating the equivalent paraboloid approximation by propagating the full field through the offset Gregorian optics using GRASP.

7 References

[1] R. Selina et al., "System Reference Design," Nat. Radio Astron. Observatory, NRAO Doc. 020.10.20.00.00-0001-REP-B-SYSTEM_REFERENCE_DESIGN, ngVLA Reference Design, Vol. 1, Jul. 2019.

[2] [Online] https://www.skatelescope.org/

[3] [Online] http://ngvla.nrao.edu/

[4] G.E. Lacy, M. Fleming, L. Baker, W. Imbriale, G. Cortes-Medellin, B. Veidt, G.J. Hovey, and D. DeBoer, "An update on the mechanical and EM performance of the composite dish verification antenna (DVA-1) for the SKA," in *Int. Conf. Electromagnetics Advanced Applications (ICEAA),* Cape Town, South Africa, Sept. 2–7, 2012.

[5] L. Baker and W. A. Imbriale, “Optical Design of DVA-1, A Prototype Antenna for the SKA Mid-Band Array,” in *16th Int. Sym. on Antenna Technology and Applied Electromagnetics (ANTEM)*, Victoria, BC, Canada, Jul. 13–16, 2014.

[6] L. B. G. Knee, L. Baker, A. Gray, G. Hovey, M. Kesteven, G. Lacy and T. Robishaw, “System performance testing of the DVA-1 radio telescope,” in *Proc. SPIE 9906, Ground-based and Airborne Telescopes VI*, 99063T, Jul. 27, 2016.

[7] M. Islam G. Lacy, “An improved secondary reflector for DVA-2 radio telescope: a case study on application of structural optimization technique,” in *Proc. SPIE 10700, Ground-based and Airborne Telescopes VII*, 107005T, Jul. 6, 2018.

[8] L. Locke, L. A. Baker, D. Henke, F. Jiang, L. B. G. Knee, V. Reshetov, “Q-band single pixel receiver development for the ngVLA and NRC,” in *Proc. SPIE 10708, Millimeter, Submillimeter, and Far-Infrared Detectors and Instrumentation for Astronomy IX*, 1070832, Jul. 9, 2018.

[9] S. Salem Hesari, D. Henke, V. Reshetov, F. Jiang, A. Seyfollahi, L. B. G. Knee, L. Baker, J. Bornemann, D. Chalmers, “Q-band receiver system design for the Canadian DVA-2 radio telescope,” in *Proc. SPIE 11453, Millimeter, Submillimeter, and Far-Infrared Detectors and Instrumentation for Astronomy X*, 114533A, Dec. 2020.

[10] K. Pontoppidan, “Electromagnetic properties and optical analysis of the ALMA antennas and front ends,” Nat. Radio Astron. Observatory, Charlottesville, VA, ALMA EDM Doc. FEND-80.04.00.00-026-A-REP, Jan. 2008.

[11] S. Salem Hesari, D. Henke, and L. B. G. Knee, “A Proposed Vacuum Window for DVA-2 Q-band Receiver and ngVLA Band-5,” submitted for publication in *URSI GASS 2021*, Rome, Aug. 28–Sept. 4, 2021.